Volume 1 | Number 1 | Jan 2013 | Pages 1–100

CrystEngComm

www.rsc.org/crystengcomm

ROYAL SOCIETY OF CHEMISTRY

This is an *Accepted Manuscript*, which has been through the Royal Society of Chemistry peer review process and has been accepted for publication.

Accepted Manuscripts are published online shortly after acceptance, before technical editing, formatting and proof reading. Using this free service, authors can make their results available to the community, in citable form, before we publish the edited article. We will replace this *Accepted Manuscript* with the edited and formatted *Advance Article* as soon as it is available.

You can find more information about *Accepted Manuscripts* in the **Information for Authors**.

Please note that technical editing may introduce minor changes to the text and/or graphics, which may alter content. The journal's standard **Terms & Conditions** and the **Ethical guidelines** still apply. In no event shall the Royal Society of Chemistry be held responsible for any errors or omissions in this *Accepted Manuscript* or any consequences arising from the use of any information it contains.

Thermal structural stability of multi-component olivine electrode for lithium ion batteries

Kyu-Young Park [†,a, b], Hyungsub Kim [†,a, c], Seongsu Lee[c], Jongsoon Kim[c], Jihyun Hong [a], Hee-Dae Lim [a, b], Inchul Park [a, b] and Kisuk Kang [a, b, *]

[a] Department of Materials Science and Engineering, Research Institute of Advanced Materials (RIAM), Seoul National University, 599 Gwanak-ro, Gwanak-gu, Seoul 151-742, Republic of Korea

[b] Center for Nanoparticle Research, Institute for Basic Science (IBS), Seoul National University, Seoul 151-742, Republic of Korea

[c] Korea Atomic Energy Research Institute, P.O. Box 105, Daejeon 305-600, Republic of Korea

[†] These authors contributed equally.

*Corresponding Author. Tel.: +82-2-880-7088 Fax.: +82-2-885-9671 E-mail address: matlgen1@snu.ac.kr

Abstract

Olivine electrodes have been extensively studied as an important class of cathode materials for lithium-ion batteries. Although $LiFePO_4$ has shown promise as a low-cost and high-power electrode thereby leading to its commercialization, recently, binary and ternary olivines such as $Li(Fe,Mn,Co)PO_4$ have also been considered as alternatives to overcome the low operating voltage and low energy density of $LiFePO_4$. Herein, we investigate the structural evolution of $Li(Mn_{1/3} Fe_{1/3}Co_{1/3})PO_4$, which is a promising multi-component olivine cathode material, using combined *in situ* high-temperature X-ray diffraction and flux neutron diffraction analyses at various states of charge. The phase stability map of the electrode shows that the de/lithiation occurs via a one-phase reaction from room temperature to ~500 °C with excellent thermal stability. Maximum entropy method analysis reveals anisotropic lattice expansion along each lattice direction at elevated temperature, which corresponds well with the lattice variations observed upon delithiation in the electrochemical cell.

Keywords

Multicomponent olivine, structure characterization, thermal phase behavior, Maximum entropy method

Introduction

LiMePO$_4$ olivine-type compounds (Me = Mn, Fe, Co, Ni) have been recently highlighted as a promising family of cathode materials for emerging large-scale energy storage devices such as those used in electric vehicles or smart grid systems.[1-3] Since the pioneering work by Goodenough and co-workers,[1, 2] extensive research has been performed to understand their intrinsic material properties and electrochemical mechanisms, which have aided in enhancing their electrochemical performance.[4-10] The general de/lithiation mechanism of LiFePO$_4$ or LiMnPO$_4$ olivine electrodes is well known to occur via a two-phase reaction;[7] however, nano-sizing[11] or multi-component substitution of the transition metals[12, 13] can affect the phase behavior, resulting in conversion of the two-phase reaction into a one-phase reaction. For example, Grey group investigated that the substitution ratio in the olivine crystal structure sensitively affects the overall delithiation mechanism during electrochemical cycling, showing distinguishable length of coherent interface and intermediate phases coexisting within or between the active particles depending on Fe/Co ratio.[14] Theoretical and experimental works have suggested that the origins of the solid-solution behavior in multi-component olivine electrodes can be explained by the electrostatic interaction between the transition metal and neighboring vacancy/Li ion and/or the internal elastic force in the olivine crystal structure.[15-18] More recently, it was also demonstrated that even in moderate-sized LiFePO$_4$ particles, a non-equilibrium path can appear during fast electrochemical cycling, resulting in the solid-solution-like behavior.[19, 20]

The phase behavior of the olivine structure can also be affected by the operating temperature. Delacourt and *et al.* systematically investigated the temperature-dependent phase evolution of Li$_x$FePO$_4$ ($0 \leq x \leq 1$), observing solid-solution behavior above ~350 °C. Moreover, two metastable phases corresponding to Li$_{0.75}$FePO$_4$ and Li$_{0.5}$FePO$_4$ were observed under cooling

processes.[5] In contrast, Li_xMnPO_4 or Li_xCoPO_4 olivine ($0 < x < 1$) did not exhibit any signature of the solid-solution behavior even at elevated temperature and underwent phase decomposition below ~200 °C, which is attributed to the poor thermal stability of the delithiated phases.[21-23] For the Fe–Mn binary olivine, the thermal structural evolution was sensitively affected by the Fe/Mn ratio. Although all the binary olivines exhibited the one-phase behavior upon heating, the Mn-rich binary compound required higher temperature to convert from the two-phase to one-phase and decomposed at relatively lower temperature than the Fe-rich compounds.[24] All the previous studies imply that a close correlation exists between the intrinsic thermal stability and composition of transition metals in the olivine crystal.

The purpose of this work is to further explore the correlation between the thermal phase evolution and transition metal compositions at elevated temperature for the ternary multi-component olivine. The ternary multi-component olivines have been considered as alternatives to overcome the intrinsic problems of single metal component olivines, such as low energy density of $LiFePO_4$, slow kinetics of $LiMnPO_4$ and poor cycle-stability of $LiCoPO_4$, because the substitution of olivine metal compound could make a counterbalance to each metal composition's intrinsic properties.[12, 15, 16] Despite promising electrochemical properties of ternary multi-component olivine, it is still unclear on the thermal stability and phase evolution. We use the one-third $Li(Mn_{1/3}Fe_{1/3}Co_{1/3})PO_4$ olivine as a model system, the phase stability map of the electrode is constructed through combined high-temperature X-ray diffraction (XRD) and neutron diffraction (ND) analyses. The phase evolution of one-third olivine is demonstrated to occur via a solid-solution for the temperature range between 25 °C to ~500 °C with excellent thermal stability, suggesting that even the relatively small portion of Fe ions could reinforce the thermal stability of the olivine crystal at delithiated states.

Maximum entropy method (MEM) analysis, which has been demonstrated to be capable of directly visualizing precise thermal atomic motion in a crystal structure,[25, 26] reveals that Li nuclear densities along the [010] diffusion path are connected at relatively low temperature of 100 °C, strongly suggesting that the multi-transition metal components can facilitate the solid-solution behavior in the olivine structure. Also, we observe that the anisotropic thermal lattice expansion occurs under the thermal-driven solid-solution range, which coincides with the lattice variations of olivine crystals exhibited during the de/lithiation in the room-temperature electrochemical cell. The origin of the anisotropic thermal property is elucidated with respect to the oxygen framework thermal vibration module using neutron-based Rietveld refinement and MEM analysis.

Experimental section

1. Sample preparation

The metal precursors of the multi-component olivine were synthesized via the co-precipitation method to prevent local metal segregation.[27] Stoichiometric amounts of $MnSO_4 \cdot H_2O$ (99 %, Aldrich), $(NH_4)_2Fe(SO_4)_2 \cdot 7H_2O$ (99 %, Aldrich), $CoSO_4 \cdot 7H_2O$ (99 %, Aldrich), and $(NH_4)_2C_2O_4 \cdot H_2O$ (99 %, Aldrich) (1:1:1:1 molar ratio) were used for the co-precipitation. First, 0.7 M ammonium oxalate aqueous solution and 0.5 M mixed metal precursors were prepared; then, the mixed metal solution was added dropwise into the oxalate aqueous solution in an Ar-filled glove box over 6 h at 90 °C. The precipitate powder was filtered and dried at 120 °C for 2 h. The $Li(Mn_{1/3}Fe_{1/3}Co_{1/3})PO_4$ olivine was synthesized via a solid-state reaction method using the prepared mixed metal oxalate source and LiH_2PO_4 (98 %, Aldrich), which were mixed (1:1 molar ratio) by wet ball milling for 24 h in acetone. After drying at 70 °C in an oven, the mixture was heated at 350 °C under Ar for 10 h. The

powder was calcinated again at 600 °C under Ar for 10 h after pelletizing under 200 kg cm^{-2}.

Partially delithiated olivine samples were prepared via chemical delithiation using NO_2BF_6. A stoichiometric amount of NO_2BF_6 and the as-prepared multi-component olivine were mixed (molar ratios of 0.33:1, 0.50:1 0.67:1, and 1:1) in acetonitrile solution under Ar; then, the mixtures were stirred for 4 h. After the chemical delithiation, the powders were washed with acetonitrile and then dried in a 70 °C oven for 24 h.

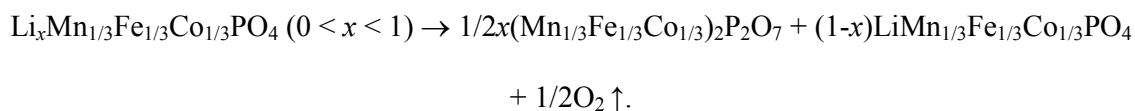## 2. Sample characterization

The stoichiometry of the delithiated compound was confirmed using inductively coupled plasma mass spectroscopy (ICP-MS, HP 4500). Thermogravimetric analysis (TGA) and differential scanning calorimetry (DSC) analysis were simultaneously performed up to 700 °C at a rate of 5 °C/min under Ar flow condition. High-temperature XRD patterns of the prepared one-third olivine were measured under Ar conditions at a heating rate of 1 °C/min (Rigaku, D/maz-2500) with a step size of 0.01 and 2θ range of 15–55°. ND patterns were obtained using a high-resolution powder diffractometer (HRPD) at the High-Flux Advanced Neutron Application Reactor (HANARO) facility at the Korea Atomic Energy Research Institute (KAERI). The measurement was performed with a step size of 0.05, 2θ range of 0–180°, and wavelength of 1.84333 λ supplied by a Ge (311) single-crystal monochromator. The *in situ* ND analyses at high temperature were performed under vacuum condition with a heating rate of 1 °C/min. The Rietveld refinement of $Li_xMn_{1/3}Fe_{1/3}Co_{1/3}PO_4$ (x = 1, 0.67, 0.5, 0.33, 0) powder samples was conducted using the Fullprof program,[28] and the fitted data were reanalyzed using Dysnomia for the MEM analyses.[29] Visualization of the nuclear densities was performed using the VESTA program.[30]

Results and discussion

Multi-component olivine samples with various delithiated phases, $Li_xMn_{1/3}Fe_{1/3}Co_{1/3}PO_4$ (x =1, 2/3, 1/2, 1/3, 0), were prepared to evaluate the thermal stability and construct a phase stability map. The lithium contents of the delithiated phases agreed well with the target compositions of the $Li_xMn_{1/3}Fe_{1/3}Co_{1/3}PO_4$ (x = 2/3, 1/2, 1/3, 0) phases, as confirmed by ICP-MS analyses (see Table S1), and its basic electrochemical performance was consistent with the previous report.[12] (See Fig. S1.) Fig. 1(a) presents the XRD patterns of the samples ($Li_xMn_{1/3}Fe_{1/3}Co_{1/3}PO_4$ (x = 1, 2/3, 1/2, 1/3, 0)), which exhibit the characteristic olivine crystal structure with the orthorhombic *Pnma* space group without any detectable crystalline impurities. In contrast to the previous cases of $LiFePO_4$ or $LiMnPO_4$, a continuous shift of major peaks was observed upon Li extraction, indicating the solid-solution behavior of $Li_xMn_{1/3}Fe_{1/3}Co_{1/3}PO_4$ at room temperature. The Rietveld refinement of the XRD patterns indicate that the a and b lattice parameters and cell volume linearly decrease upon delithiation, whereas the c lattice parameter increases, as observed in Fig. 1(b), which is consistent with previous reports.[12, 16] Note that the variation of the a lattice parameter is significantly greater than that of the b or c lattice parameter, which will be further discussed later.

The thermal stability of the $Li_xMn_{1/3}Fe_{1/3}Co_{1/3}PO_4$ (x = 1, 2/3, 1/3, 0) samples was investigated using TGA/DSC, and the results are presented in Fig. S2. All the samples were observed to be stable up to 520 °C without noticeable weight reduction or heat flow, and exothermic peaks were observed at approximately 500 °C. The origin of the exothermic reaction can be elucidated based on the *in situ* high-temperature XRD measurements shown in Figs. 2(a–d). In the cases of partially delithiated phases (Figs. 2(a–c)), additional peaks corresponding to the $Me_2P_2O_7$ phase (Me = Fe, Mn, or Co; mixed) begin to appear at approximately 520 °C, and there is no significant change except for the shift of peaks due to

the thermal expansion. Based on the XRD phase analysis, the decomposition of partially

delithiated phases occurring at 520 °C is expected to follow the reaction path:

$$Li_xMn_{1/3}Fe_{1/3}Co_{1/3}PO_4 (0 < x < 1) \rightarrow 1/2x(Mn_{1/3}Fe_{1/3}Co_{1/3})_2P_2O_7 + (1-x)LiMn_{1/3}Fe_{1/3}Co_{1/3}PO_4$$

$$+ 1/2O_2 \uparrow.$$

Compared with the partially delithiated phases, the fully delithiated phase, *i.e.,*

$Mn_{1/3}Fe_{1/3}Co_{1/3}PO_4$, was observed to decompose at a relatively lower temperature of

approximately 320 °C in Fig. 2(d). The $Mn_{1/3}Fe_{1/3}Co_{1/3}PO_4$ phase starts to lose its

crystallinity and decomposes into $(Mn_{1/3}Fe_{1/3}Co_{1/3})_3(PO_4)_2$ at 320 °C. However, this

decomposition route involves an imbalance in the stoichiometry of the metal to P ratio. Thus,

a P-rich amorphous phase is expected to be formed simultaneously during the decomposition,

which was similarly observed in previous studies on binary Fe–Mn olivine phases.[24] Upon

heating to temperatures above 520 °C, the $(Mn_{1/3}Fe_{1/3}Co_{1/3})_2P_2O_7$ phase appeared at the

expense of the $(Mn_{1/3}Fe_{1/3}Co_{1/3})_3(PO_4)_2$ phase. Accordingly, the decomposition reaction of the

$Mn_{1/3}Fe_{1/3}Co_{1/3}PO_4$ phase can be described as follows:

$$2Mn_{1/3}Fe_{1/3}Co_{1/3}PO_4 \rightarrow 2/3(Mn_{1/3}Fe_{1/3}Co_{1/3})_3(PO_4)_2 + \text{P-rich amorphous phase at } 320 °C \rightarrow$$

$$(Mn_{1/3}Fe_{1/3}Co_{1/3})_2P_2O_7 + 1/2O_2 \uparrow.$$
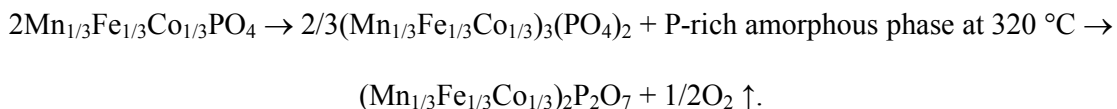
Based on the *in situ* high-temperature XRD results, the thermal phase diagram of

$Li_xMn_{1/3}Fe_{1/3}Co_{1/3}PO_4$ could be constructed as a function of Li content, as shown in Fig. 2(e).

The solid-solution phases of the delithiated $Li_xMn_{1/3}Fe_{1/3}Co_{1/3}PO_4$ ($0 < x < 1$) are maintained

up to 500 °C without phase decomposition, which is a significantly higher temperature than

those for Li_xMnPO_4 or Li_xCoPO_4 and is comparable to the thermal stability of Li_xFePO_4.[5, 21-

23] Although the fully charged phase, $Mn_{1/3}Fe_{1/3}Co_{1/3}PO_4$, decomposes at a relatively lower

temperature (~320 °C) than the $FePO_4$ phase (~500 °C),[5] the decomposition temperature is

comparable to that of binary $Fe_{1-x}Mn_xPO_4$ ($0 \leq x \leq 1$) and higher than that of Co- or Mn-based

single-component olivine materials (~200 °C).[21-23] This finding clearly suggests that the

partial occupation of Fe in the olivine enhances the thermal stability of the olivine crystal at delithiated states.

The thermal expansion coefficients of the lattice parameters were extracted from the XRD results for each $Li_xMn_{1/3}Fe_{1/3}Co_{1/3}PO_4$ (x = 1, 2/3, 1/2, 1/3, 0) and are tabulated in Table 1. (The change of the lattice parameter as a function of temperature is plotted in Figs. S3 and S4.) When the lithium content is full in the olivine, the thermal expansions are almost comparable in the a, b, and c directions, even though the elongation along the a direction is slightly higher. However, the thermal coefficients in the a and b directions display remarkable increases with decreasing lithium content compared with that in the c direction. When the olivine is fully delithiated, the thermal expansion is nearly five times larger along the a direction than along the c direction. The thermal expansion along the b direction is also nearly twice as large as that along the c direction. It is noteworthy that the variation in thermal expansion coefficient as a function of Li content coincides with the lattice parameter change during the electrochemical cycling. According to previous studies, olivine-type electrodes generally exhibit anisotropic structure evolution with larger variation in the a and b lattice parameters during cycling, which results in the large mismatch in the a and b directions between Li-rich and Li-poor phases; in contrast, the c lattice parameter does not change significantly with the electrochemical reaction.[3, 7, 13, 16] This finding indicates that the bonding nature along the a- and b- axes is relatively softer and significantly affected by the presence of lithium in the crystal structure.

The origin of the anisotropic thermal lattice expansion properties of the olivine was investigated using ND analysis. High-flux neutrons generated from reactor sources with a constant wavelength of 1.834333 Å were used to analyze the atomic positions and thermal parameters of Li, Mn, Fe, Co, P, and O ions in the structure. We applied an anisotropic

thermal motion model for Li, P, and O upon Rietveld refinement to evaluate the atomic thermal behavior, whereas each transition metal (Mn, Fe and Co) was assumed to be isotropic for the simplicity of analysis. The schematic representation of $LiMn_{1/3}Fe_{1/3}Co_{1/3}PO_4$ derived from the refinement is presented in Fig. 3. Note that Li undergoes anisotropic thermal vibration along the [010] direction at room temperature in Fig. 3(b), which is consistent with previous reports.[7, 25] In addition, the anisotropic thermal parameters of P and O atoms are similar to those of $LiFePO_4$, indicating that these properties are characteristic of the olivine crystal[7] (see supplementary Table S2). Fig. 3(c) presents magnified images of FeO_6 and PO_4 polyhedra and neighboring Li in the *ab* and *ac* planes, which are denoted by the blue dashed circle in Fig. 3(b). The black arrows in Fig. 3(c) indicate the direction and magnitude of the atomic vibration, and their comparison in each *ab* and *ac* plane clearly indicates the preferentially oriented atomic vibration. The O1, O2, and O3 oxygen ions are mainly vibrating along the *a*- and *b*-axes, whereas the motion along the *c*-axis is substantially smaller at room temperature. In addition, the vibration of Li ions is more significant in the *ab* plane than in the *ac* plane, which is consistent with the trend of the thermal lattice expansion coefficients. Rietveld refinement of the partially charged samples, $Li_xMn_{1/3}Fe_{1/3}Co_{1/3}PO_4$ (*x* = 2/3, 1/2, 1/3), reveals similar anisotropic thermal vibration of the O1, O2, and O3 ions as that observed for the as-prepared $LiMn_{1/3}Fe_{1/3}Co_{1/3}PO_4$, as demonstrated in Table S2 and Figs. S5 (a–c).

The strong thermal vibration along the *a*- and *b*-axes of oxygen ions was also confirmed by MEM analysis, which has been demonstrated to be an efficient method to visualize dynamic atomic thermal motion in a crystal structure.[25, 26] In particular, the anisotropic atomic thermal motion of light elements such as Li, P, and O can be precisely estimated. Fig. S6 presents a 3D nuclear density map of $Li_xMn_{1/3}Fe_{1/3}Co_{1/3}PO_4$ (*x* = 1, 2/3, 1/2, 1/3) at room temperature

obtained from the MEM analysis. An anisotropic nuclear density of Li along the [010] direction is clearly observed, and the anisotropic thermal motions of Li, P, and O agree well with those observed based on the Rietveld refinement (see Figs. S5 and S6). The high-temperature atomic thermal behavior was further evaluated using temperature-dependent MEM analysis. For the enhanced Li dynamics in the structure, we used partially delithiated $Li_{2/3}Mn_{1/3}Fe_{1/3}Co_{1/3}PO_4$ samples.[25] Fig. 4(a) presents the ND patterns of $Li_{2/3}Mn_{1/3}Fe_{1/3}Co_{1/3}PO_4$ at 25 °C, 100 °C, and 200 °C with the points indicated in the inset thermal phase diagram. As expected from the *in situ* high-temperature XRD analyses, the solid-solution phases of $Li_{2/3}Mn_{1/3}Fe_{1/3}Co_{1/3}PO_4$ were well maintained. Notably, the Li nuclear densities are connected to each other along the [010] direction with a sinusoidal motion at 100 °C and 200 °C (see Fig. 4(b)). Note that Li connection was observed at relatively lower temperature (below 200 °C) compared with the previous report on $LiFePO_4$,[25] which might be attributed to an increased tendency for solid-solution behavior in the multi-component olivine structure. The 2D nuclear density maps in Fig. S7 also provide clear evidence of the 1D Li diffusion along the [010] direction. Furthermore, through the visualization of atomic thermal vibration motion, we can confirm that most of the nuclear densities observed as an anisotropic ellipsoid are parallel to the *a*- and *b*- axes. The O ions exhibit strong thermal vibration along the *a*- and *b*-axes, as observed in Fig. 4 (c), and the Li ions form a particularly strong anisotropic ellipsoid parallel to the *b*-axis. The anisotropic thermal motion and contour size increase along the *a*- and *b*-axes as the temperature increases, indicating larger thermal expansion along those directions. This detailed picture of the atomic motion explains the variations in the thermal coefficient of each axis (Table 1). Furthermore, the bonding nature along each lattice direction inferred from the thermal behavior also hints at the origin of the anisotropic structure evolution during delithiation of olivine materials.

Conclusion

In this work, we investigated the structural evolution of a multi-component olivine electrode, which is one of the important class of electrode materials, at elevated temperatures using combined *in situ* XRD and ND analyses and constructed a thermal phase diagram. The fully/partially delithiated multi-component olivine exhibited superior thermal stability compared with Co- or Mn-based single-component olivine materials, suggesting that partial occupation of Fe in the olivine enhances the thermal stability of the olivine crystal. Investigation of the variations of the lattices with temperature revealed anisotropic thermal expansion along each lattice direction. Precise Rietveld refinement and MEM visualization suggested that the anisotropy is strongly related to oxygen atomic vibration preferentially occurring in the *a* or *b* directions. Moreover, we observe that the thermally driven Li ion hopping along the [010] direction is facilitated at the partially delithiated one-third olivine, suggesting that the multi-transition metal nature can enhance the Li ion diffusion in the olivine crystal structure. We expect that a thermal stability map and detailed thermal structural characterization at the atomic level of multi-component olivines would provide a clearer understanding of the olivine crystal structure.

References

1. A. K. Padhi, K. S. Nanjundaswamy and J. B. Goodenough, *J. Electrochem. Soc.*, 1997, **144**, 1188.

2. A. K. Padhi, K. S. Nanjundaswamy, C. Masquelier, S. Okada and J. B. Goodenough, *J. Electrochem. Soc.*, 1997, **144**, 1609.

3. Y. Wang, P. He and H. Zhou, *Energ. Environ. Sci.*, 2011, **4**, 805.

4. D. Morgan, A. Van der Ven and G. Ceder, *Electrochem. Solid. St.*, 2004, **7**, A30.

5. C. Delacourt, P. Poizot, J.-M. Tarascon and C. Masquelier, *Nat. Mater.*, 2005, **4**, 254.

6. B. Kang and G. Ceder, *Nature*, 2009, **458**, 190.

7. A. Yamada, H. Koizumi, S.-i. Nishimura, N. Sonoyama, R. Kanno, M. Yonemura, T. Nakamura and Y. Kobayashi, *Nat. Mater.*, 2006, **5**, 357.

8. S.-Y. Chung, J. T. Bloking and Y.-M. Chiang, *Nat. Mater.*, 2002, **1**, 123.

9. C. Delmas, M. Maccario, L. Croguennec, F. Le Cras and F. Weill, *Nat. Mater.*, 2008, **7**, 665.

10. G. Chen, X. Song and T. J. Richardson, *J. Electrochem. Soc.*, 2007, **154**, A627.

11. P. Gibot, M. Casas-Cabanas, L. Laffont, S. Levasseur, P. Carlach, S. Hamelet, J.-M. Tarascon and C. Masquelier, *Nat. Mater.*, 2008, **7**, 741.

12. H. Gwon, D.-H. Seo, S.-W. Kim, J. Kim and K. Kang, *Adv. Funct. Mater.*, 2009, **19**, 3285.

13. A. Yamada, Y. Kudo and K.-Y. Liu, *J. Electrochem. Soc.*, 2001, **148**, A1153.

14. F. C. Strobridge, H. Liu, M. Leskes, O. J. Borkiewicz, K. M. Wiaderek, P. J. Chupas, K. W. Chapman and C. P. Grey, *Chem. Mater.*, 2016, **28**, 3676-3690.

15. D.-H. Seo, H. Gwon, S.-W. Kim, J. Kim and K. Kang, *Chem. Mater.*, 2009, **22**, 518-523.

16.   K.-Y. Park, J. Hong, J. Kim, Y.-U. Park, H. Kim, D.-H. Seo, S.-W. Kim, J.-W. Choi and K. Kang, *J. Electrochem. Soc.*, 2013, **160**, A444.

17.   D. A. Cogswell and M. Z. Bazant, *ACS Nano*, 2012, **6**, 2215.

18.   P. Bai, D. A. Cogswell and M. Z. Bazant, *Nano Lett.*, 2011, **11**, 4890.

19.   R. Malik, F. Zhou and G. Ceder, *Nat. Mater.*, 2011, **10**, 587.

20.   W. Dreyer, J. Jamnik, C. Guhlke, R. Huth, J. Moskon and M. Gaberscek, *Nat. Mater.*, 2010, **9**, 448.

21.   S. P. Ong, A. Jain, G. Hautier, B. Kang and G. Ceder, *Electrochem. Commun.*, 2010, **12**, 427.

22.   N. N. Bramnik, K. Nikolowski, D. M. Trots and H. Ehrenberg, *Electrochem. Solid. St.*, 2008, **11**, A89.

23.   S.-W. Kim, J. Kim, H. Gwon and K. Kang, *J. Electrochem. Soc.*, 2009, **156**, A635.

24.   J. Kim, K.-Y. Park, I. Park, J.-K. Yoo, J. Hong and K. Kang, *J. Mater. Chem.*, 2012, **22**, 11964.

25.   S.-i. Nishimura, G. Kobayashi, K. Ohoyama, R. Kanno, M. Yashima and A. Yamada, *Nat. Mater.*, 2008, **7**, 707.

26.   M. Yashima, M. Itoh, Y. Inaguma and Y. Morii, *J. Am. Chem. Soc.*, 2005, **127**, 3491.

27.   Y.-U. Park, J. Kim, H. Gwon, D.-H. Seo, S.-W. Kim and K. Kang, *Chem. Mater.*, 2010, **22**, 2573.

28.   J. Carvajal, *Abstracts of the Satellite Meeting on Powder Diffraction of the XV Congress of the International Union of Crystallography, Toulouse, France*, 1990, p.127.

29.   F. Izumi and K. Momma, *IOP Conference Series: Materials Science and Engineering*, 2011, **18**, 022001.

30.   K. Momma and F. Izumi, *J. Appl. Crystallog.*, 2011, **44**, 1272-1276.

Acknowledgements

Figure captions
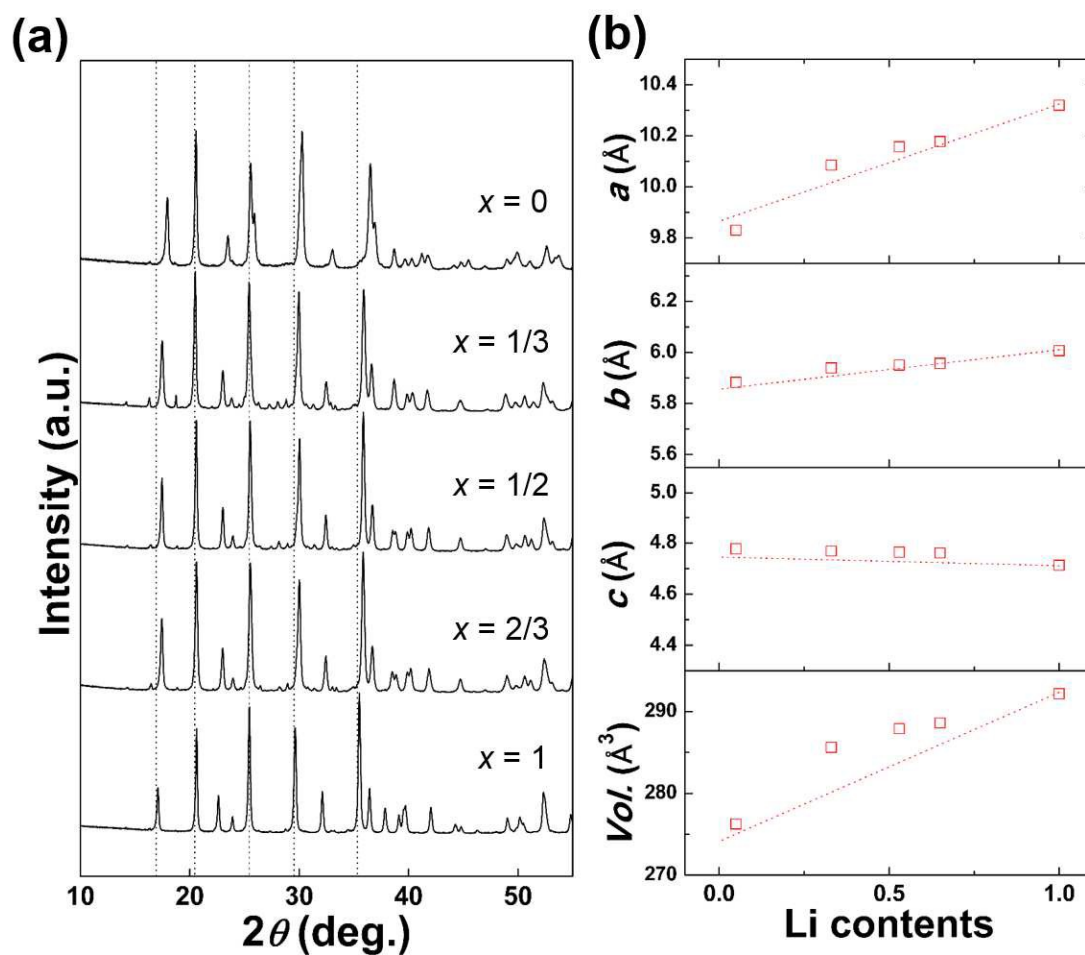
Figure 1.

Fig. 1. (a) XRD patterns of the $Li_xMn_{1/3}Fe_{1/3}Co_{1/3}PO_4$ (x = 1, 2/3, 1/2, 1/3, 0). (b) Lattice parameters and cell volume of prepared samples confirmed by Rietveld refinement method. The red dotted line is predicted values from Vegard's law.
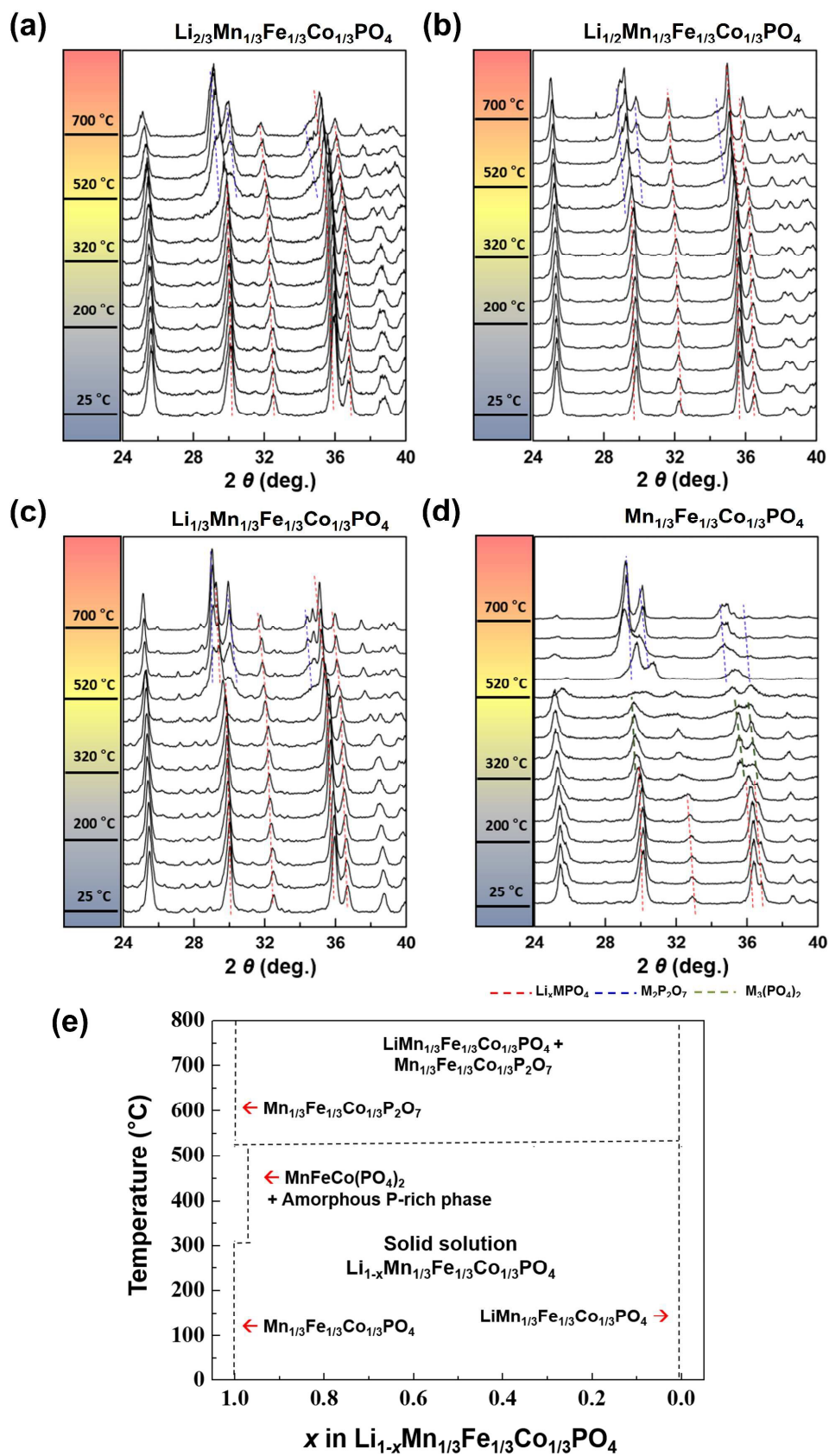
(a) Li$_{2/3}$Mn$_{1/3}$Fe$_{1/3}$Co$_{1/3}$PO$_4$

(b) Li$_{1/2}$Mn$_{1/3}$Fe$_{1/3}$Co$_{1/3}$PO$_4$

(c) Li$_{1/3}$Mn$_{1/3}$Fe$_{1/3}$Co$_{1/3}$PO$_4$

(d) Mn$_{1/3}$Fe$_{1/3}$Co$_{1/3}$PO$_4$

--- Li$_x$MPO$_4$ --- M$_2$P$_2$O$_7$ --- M$_3$(PO$_4$)$_2$

(e)

LiMn$_{1/3}$Fe$_{1/3}$Co$_{1/3}$PO$_4$ +
Mn$_{1/3}$Fe$_{1/3}$Co$_{1/3}$P$_2$O$_7$

← Mn$_{1/3}$Fe$_{1/3}$Co$_{1/3}$P$_2$O$_7$

← MnFeCo(PO$_4$)$_2$
+ Amorphous P-rich phase

Solid solution
Li$_{1-x}$Mn$_{1/3}$Fe$_{1/3}$Co$_{1/3}$PO$_4$

← Mn$_{1/3}$Fe$_{1/3}$Co$_{1/3}$PO$_4$ LiMn$_{1/3}$Fe$_{1/3}$Co$_{1/3}$PO$_4$ →

Temperature (°C)

x in Li$_{1-x}$Mn$_{1/3}$Fe$_{1/3}$Co$_{1/3}$PO$_4$

Fig. 2. *In situ* high temperature XRD patterns of $Li_xMn_{1/3}Fe_{1/3}Co_{1/3}PO_4$.((a) x = 2/3, (b) x = 1/2, (c) x = 1/3 and (d) x = 0) Red, blue and green dash line present the peaks from $Li_xMn_{1/3}Fe_{1/3}Co_{1/3}PO_4$, $M_2P_2O_7$ and $M_3(PO_4)_2$, respectively. (e) Thermal phase diagram of $Li_xMn_{1/3}Fe_{1/3}Co_{1/3}PO_4$ as a function of Li contents.

	Thermal expansion coefficient (10^{-5} Å/°C)				
Li contents	**1**	**2/3**	**1/2**	**1/3**	**0**
a lattice	12.26	15.47	20.38	32.28	39.85
b lattice	8.49	9.16	11.08	11.79	14.05
c lattice	7.41	7.94	6.72	7.60	8.36

Table 1. The thermal lattice expansion coefficients at various Li contents. The thermal coefficients are estimated from lattice parameter change during heating.
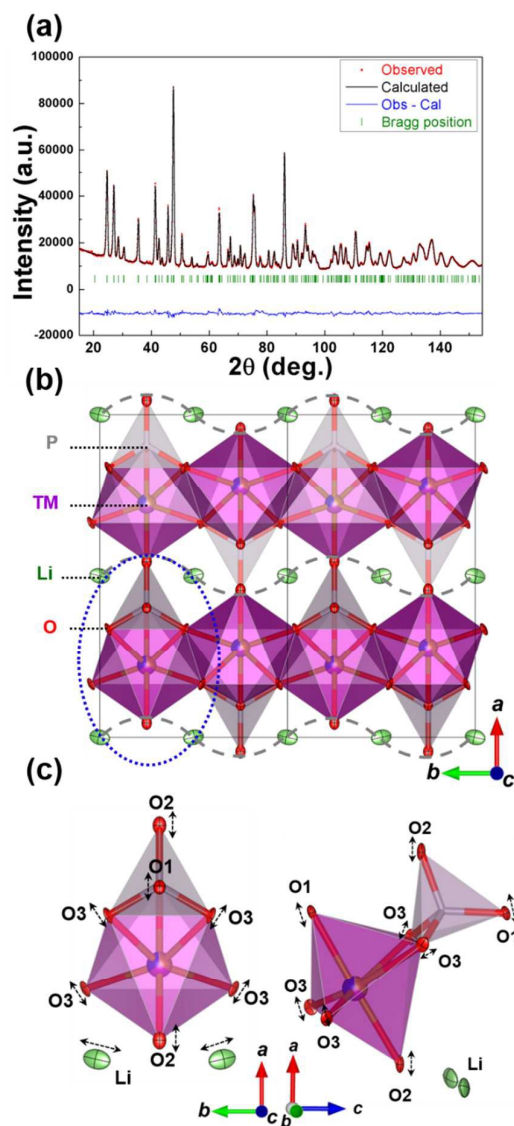
Figure 3. (a) Rietveld refinement of the neutron diffraction pattern of $LiMn_{1/3}Fe_{1/3}Co_{1/3}PO_4$ at room temperature. The observed data, calculated profiles, Bragg position and difference between observed and calculated profiles are presented as red markers, black line, green markers and blue line, respectively. (b) Structure schematics of $LiMn_{1/3}Fe_{1/3}Co_{1/3}PO_4$ from Rietveld refinement. The anisotropic thermal motion with 60 % probability of each atom is illustrated. (c) Magnified structure schematics of FeO_6 octahedral and PO_4 tetrahedral along c- and b-axes.
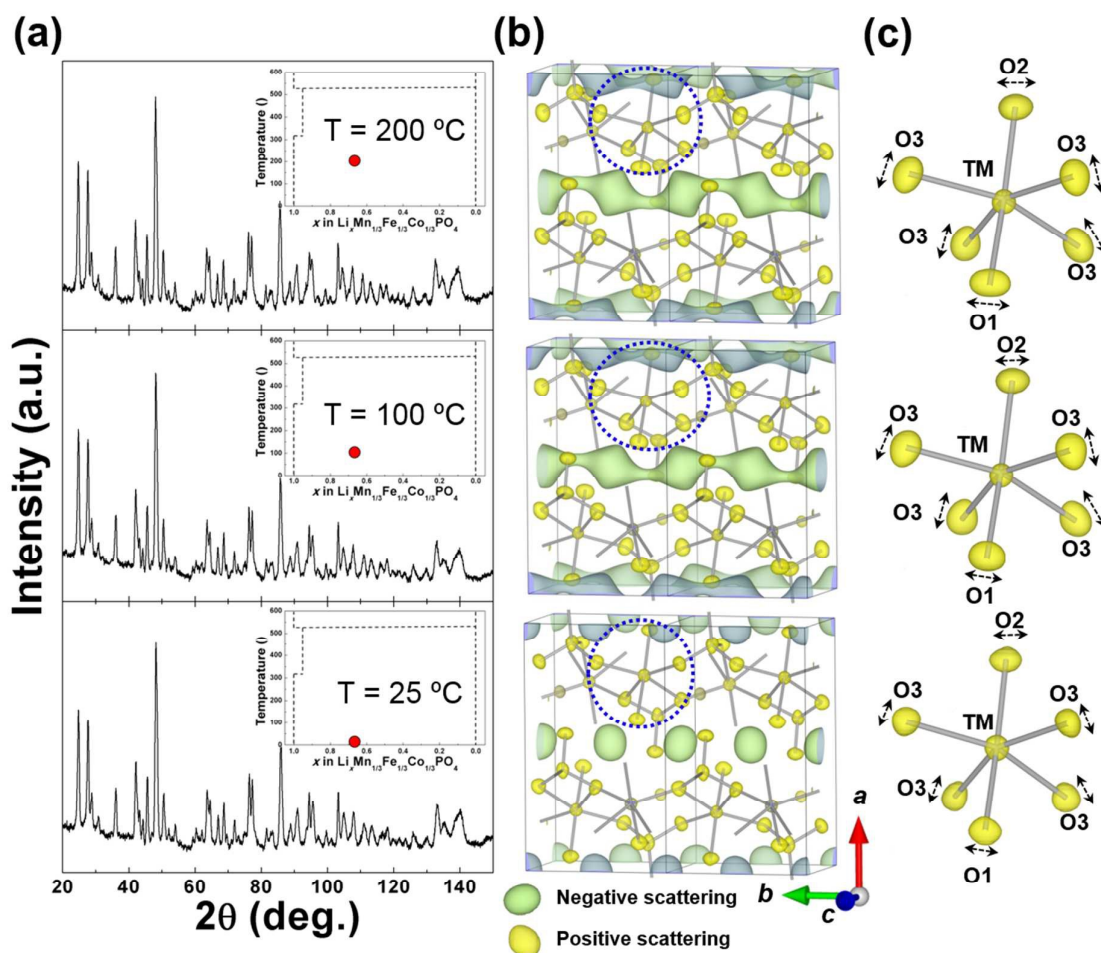
Fig. 4. (a) The neutron diffraction patterns of $Li_{2/3}Mn_{1/3}Fe_{1/3}Co_{1/3}PO_4$ at various temperatures (T = 25 °C, 100 °C and 200 °C). The inset in each figure shows the thermal phase diagram of $Li_xMn_{1/3}Fe_{1/3}Co_{1/3}PO_4$, and the measurement temperature was marked as red markers. (b) The 3D nuclear density contours of each atom from the MEM analysis. The negative scattering caused from Li nuclear density and positive scattering caused from oxygen and phosphor atoms are shown as green and yellow circles, respectively. (c) Magnified figure of TMO_6 octahedra which are marked as blue dotted line in (b).